

RESEARCH ARTICLE

Order of Magnitude Signal Gain in Magnetic Sector Mass Spectrometry Via Aperture Coding

Evan X. Chen,¹ Zachary E. Russell,¹ Jason J. Amsden,¹ Scott D. Wolter,^{1,2} Ryan M. Danell,³ Charles B. Parker,¹ Brian R. Stoner,⁴ Michael E. Gehm,¹ Jeffrey T. Glass,¹ David J. Brady¹

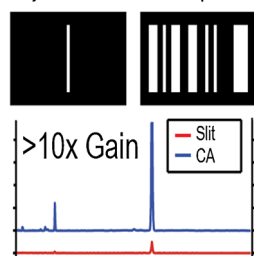
¹Department of Electrical and Computer Engineering, Duke University, Durham, NC 27708, USA

²Department of Physics, Elon University, Elon, NC 27278, USA

³Danell Consulting, Winterville, NC 28590, USA

⁴Discovery-Science-Technology Division, RTI International, Research Triangle Park, NC 27709, USA

Object Slit vs Coded Aperture



Abstract. Miniaturizing instruments for spectroscopic applications requires the designer to confront a tradeoff between instrument resolution and instrument throughput [and associated signal-to-background-ratio (SBR)]. This work demonstrates a solution to this tradeoff in sector mass spectrometry by the first application of one-dimensional (1D) spatially coded apertures, similar to those previously demonstrated in optics. This was accomplished by replacing the input slit of a simple 90° magnetic sector mass spectrometer with a specifically designed coded aperture, deriving the corresponding forward mathematical model and spectral reconstruction algorithm, and then utilizing the resulting system to measure and reconstruct the mass spectra of argon, acetone, and ethanol. We expect the application of coded apertures to

sector instrument designs will lead to miniature mass spectrometers that maintain the high performance of larger instruments, enabling field detection of trace chemicals and point-of-use mass spectrometry.

Keywords: Coded aperture sector mass spectrometry, Computational mass spectrometry, Miniature mass spectrometry, Magnetic sector mass spectrometry

Received: 3 February 2015/Revised: 3 April 2015/Accepted: 27 April 2015/Published Online: 26 June 2015

Introduction

Mass spectrometers are versatile analytical laboratory instruments because they are fast, accurate, sensitive, selective, and can accommodate a wide variety of sample types [1–4]. However, in situ measurements with mass spectrometers in field settings are difficult because of the size, cost, and complexity of the instrument. In particular, mass spectrometers based on magnetic sector mass analyzers—although noted for their high mass accuracy and resolution—have historically required large size and weight to achieve this performance, thereby limiting their use outside of the laboratory [5, 6]. Miniaturization of mass spectrometers, and magnetic sector

instruments in particular, would enable hand-held and portable instruments for in situ analysis in a variety of applications from security to environmental monitoring and health care. Although designs for miniaturized mass spectrometers have been presented [7–9], miniaturization is currently accompanied by a simultaneous decrease in performance, including resolution and throughput, thus limiting the utility of such instruments for in situ chemical analysis and identification.

In this paper, we describe the first reported demonstration of one-dimensional (1D) spatially coded apertures to sector mass spectrometry. This approach can help to minimize the performance degradation accompanying miniaturization. Similar to optical spectroscopy, the application of spatially coded apertures to sectors yields an increase in instrument throughput while maintaining the equivalent resolution of a single slit after spectral reconstruction. This results in a significant increase in signal-to-background-ratio (SBR) and, thus, lowers detection limits (i.e., increased sensitivity to trace analytes), which will enable practical magnetic sector miniaturization. Increased throughput is also desirable for conventional instruments (i.e., large laboratory instruments) for applications that require high

Evan X. Chen and Zachary E. Russell contributed equally to this work.

Electronic supplementary material The online version of this article (doi:10.1007/s13361-015-1178-y) contains supplementary material, which is available to authorized users.

Correspondence to: Jeffrey Glass; e-mail: jeff.glass@duke.edu

analyte utilization, such as when limited sample volumes are available. Recently, we demonstrated spatially two-dimensional (2D) coded apertures [10] in a magnetic sector mass spectrometer. The current work using 1D apertures shows increased throughput compared with the 2D apertures because of elimination of aperture fabrication constraints discussed in the 2D coding demonstration. Furthermore, while the 2D system requires 2D detection capability (such as provided by an MCP, phosphor screen, and digital camera combination), the 1D coding scheme is compatible with recently developed 1D ion detector arrays [11, 12]. This will allow for easier implementation in eventual fieldable units.

Spatially coded apertures have been primarily used in optical imaging and spectroscopy systems [13]. In dispersive optical coded aperture spectroscopy, a throughput gain of greater than 10X was achieved with an equivalent resolution compared with a conventional single slit approach [14, 15]. Although spatial coding techniques for mass spectrometry have been hypothesized [16], to our knowledge they have not been demonstrated until recently [10]. Temporal coding has been utilized in time-of-flight mass spectrometry (TOF MS). The use of Hadamard transforms results in extension of the ion duty cycle up to 100% with an accompanying significantly higher throughput compared with conventional TOF MS [17–19]. Hadamard transforms have also been successfully utilized in tandem Fourier transform ion cyclotron resonance (FT-ICR) mass spectrometry [20]. By encoding the parent ion accumulation time, the iterative accumulation multiplexing (IAM) technique was demonstrated on an FT-ICR mass spectrometer [21]. In addition, a quadrupole ion trap-based multi-resonant frequency excitation (mRFE) ejection compressive mass analysis technique has been developed in our lab. This mRFE method can reduce mass analysis time by a factor of three to six without losing spectral specificity for chemical classification purposes [22].

Mass spectrometers employing sector mass analyzers are analogous to optical spectrometers in that they both contain a spatial filter, dispersive element, and detector. In both cases, the spatial filter is traditionally provided by the resolution-defining slit. Furthermore, the fields (both electric and magnetic) of a sector mass analyzer are dispersive elements and are thus analogous to the diffraction grating in dispersive optical spectroscopy. Finally, in both domains, a detector is placed after the dispersive element. Building on this analogy between optical spectroscopy and magnetic sector mass spectrometry, we have constructed a simple magnetic sector mass spectrometer where we replace the slit spatial filter with a coded aperture in order to demonstrate the advantages of coding.

In this manuscript, we report on our derivation of a mathematical forward model for our custom built 90° magnetic sector system (hereafter referred to as a 90° MS). Based on some initial known compound measurements, we carefully calibrate our system forward model such that it corresponds to the 90° MS with sufficient accuracy. Based on this explicit forward model, we formulate an algorithm to reconstruct mass spectra from ion intensity versus detector position data measured in our

90° MS. We measure this ion intensity for a range of concentrations of argon, ethanol, and acetone using spatially coded apertures of varying complexity, and compare the reconstructed spectra with measurements made using a single slit. We show that the use of 1D coded apertures can produce more than an order of magnitude increase in throughput and an accompanying increase in SBR with no decrease in instrument resolution.

Aperture Coding Model

There are numerous physical approaches to the separation of molecules as a function of their mass as manifested in different types of mass spectrometers, including ion trap [23–25], time of flight [26–28], FT-ICR [29–31], and sector-based instruments [32–38]. Here, we focus on a subset of sector-based instruments that provide simultaneous analysis across the entire mass range of interest, as dispersed onto a single focal plane. These instruments are often referred to as spectrographs [39], and geometries include the Mattauch-Herzog [35], Bainbridge-Jordan [37], or Bleakney-Hipple [38], as well as sector mass analyzers containing only magnetic fields [32, 34, 40] that lack double focusing properties. In all of these sectors, the mass spectra are measured by passing an ion beam through a mass analyzer that uses electric and/or magnetic fields to disperse the ions spatially according to their mass-to-charge ratio. The resulting spatial distribution is then recorded by a detector array. When using a single slit to spatially define the ion beam, a simple calibration to a few known ion peaks is all that is required to reconstruct a mass spectrum from the pattern recorded at the detector. However, multiple slits can be implemented in order to enhance the instrument throughput. In this case, the detected signal is a combination of the ions passing through each slit. The end result is a multiplexed measurement requiring an accurate mathematical model to reconstruct the mass spectrum from the complex spatial pattern produced at the detector. The multiple slits are designed in a specific way to encode the ion signal and allow for a well-conditioned reconstruction; therefore, they are termed coded apertures (examples are shown in Figure 1a).

Forward Model Derivation

The forward model is a mathematical representation of the mass spectrometer system that can be used to calculate the pattern of ions on the detector plane from the pattern of the aperture and the physical characteristics of the system. A thorough derivation of the forward model which is applicable to both this manuscript and the 2-D coding in Reference [10] is shown in the [Supporting Information \(SI\)](#). For convenience, in this section we present an abbreviated version of the forward model derivation. For notational simplicity, in the forward model we use α to represent m/z , the ratio of the ion mass (in u) to the net number of elementary charges. The coordinate system used in this derivation defines the x and y coordinates as

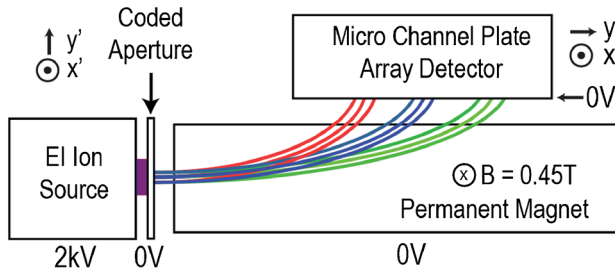
(a) Cyclic-S Spatially Coded Aperture Patterns**(b) Experimental Setup**

Figure 1. Cyclic S coded apertures and 90° magnetic sector schematic. **(a)** Five Cyclic S codes with orders of 1, 7, 11, 15, and 23 are used in this research. Details on their fabrication can be found in the [Supporting Information](#). **(b)** Schematic of the experimental set-up to confirm the benefits of spatial aperture coding in magnetic sector mass spectrometers. The apparatus consists of an electron ionization (EI) ion source, a coded aperture, a permanent magnet, and a micro channel plate (MCP) array detector. The red, green, and blue traces correspond to ions of different mass-to-charge ratio and the multiple traces at each color represent ions passing through different openings in the coded aperture. For simplicity, two local coordinate systems were used to describe the system: one on the plane of the coded aperture (x' , y'), and one on the detector plane (x , y). These are labeled above and correspond to the coordinates used in the general proof found in the [Supporting Information \(SI\)](#)

the non-mass-dispersive direction and the mass-dispersive direction in the detector plane, respectively, and the x' and y' coordinates are the spatial dimensions of the coded aperture, as shown in [Figure 1b](#). The ion intensity at a point (x, y) on the detector plane, is $g(x, y)$:

$$g(x, y) = \int f(\alpha) T(x, y, \alpha) d\alpha. \quad (1)$$

Where $f(\alpha)$ is the mass spectrum, and $T(x, y, \alpha)$ is the system transfer function, which can be defined as:

$$T(x, y, \alpha) = \iint I(x', y') t(x', y') h(x, x', y, y', \alpha) dx' dy'. \quad (2)$$

This system transfer function T describes how ions at each α travel from the coded aperture to the detector. $I(x', y')$ is the ion beam intensity spatial profile at (x', y') in the coded aperture plane, $t(x', y') \in \{0, 1\}$ is the coded aperture transmission function describing the shape of the aperture, and $h(x, x', y, y', \alpha)$ is a

kernel describing propagation through the spectrometer for an ion of specific α .

For the 90° system geometry we used in our experiment the propagation kernel h can be approximated as (see SI for a detailed derivation):

$$h(x, x', y, y', \alpha) \approx \delta \left(x - x', y - \sqrt{\frac{\sqrt{8U\alpha}(u/e)}{B}} y' - y'^2 \right). \quad (3)$$

where B is the magnitude of the applied magnetic field, U is the applied ion acceleration voltage, and (u/e) is the ratio of a u to an elementary charge in the desired set of physical units.

After discretizing $g(x, y)$ with two-dimensional rect function and $f(\alpha)$ with one-dimensional delta function, the mathematical system forward model can be represented as the linear system:

$$g = Hf. \quad (4)$$

where g is a vector of experimentally measured data and H is the forward matrix which maps the mass spectrum f to the measurement data vector. Using the above discretized forward model with a Poisson maximum likelihood estimation reconstruction algorithm [10, 41], we can estimate the desired mass spectrum f from the measurements g .

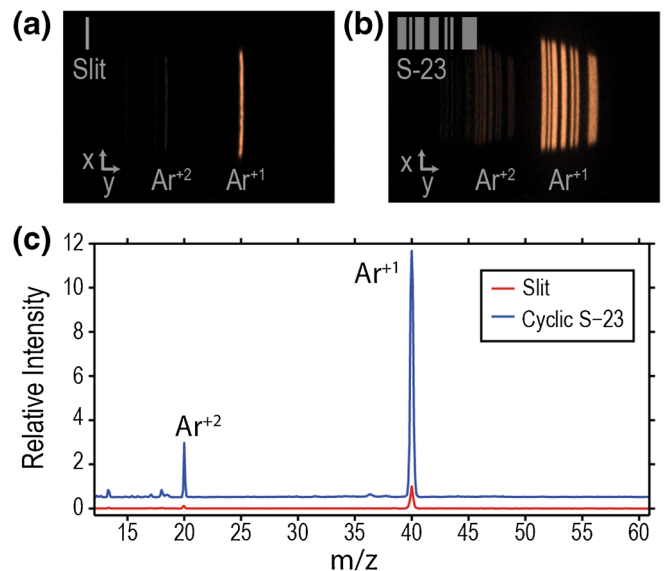


Figure 2. Detector images and reconstructed spectra for argon used in the forward model calibration. **(a)** Unprocessed image at the detector plane using single slit. The images are $40 \text{ mm} \times 10 \text{ mm}$. **(b)** Unprocessed image at the detector plane using the Cyclic S-23 coded aperture. **(c)** Reconstructed argon spectra using Cyclic S-23 and slit apertures, where the Cyclic S-23 spectrum is arbitrarily shifted by 0.5 relative intensity units for clarity. The reconstructed mass spectra are normalized such that the slit argon $m/z = 40$ peak has an intensity of 1 unit

Forward Model Calibration

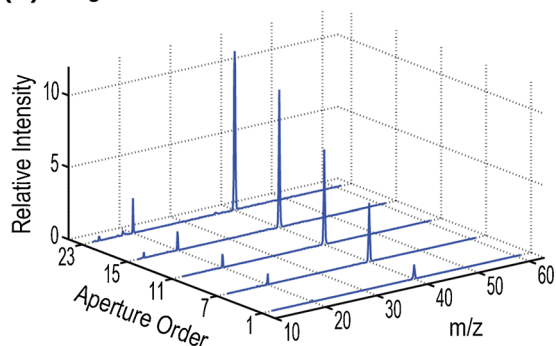
Figure 2 shows examples of the spatial pattern produced at the detector for argon gas for both the (a) slit and (b) S-23 coded apertures. There are two major features in the argon data resulting from singly and doubly ionized argon at $m/z = 40$ and $m/z = 20$, respectively. Note that although the S-23 coded aperture is rectangular, the image exhibits a keystone shape. We attribute this shape to the non-uniform magnetic field produced by the bar magnet. As a result of this non-uniformity, ions that pass through different parts of the coded aperture encounter slightly different field magnitudes and directions along their trajectories. In addition, the image of the aperture pattern is magnified. There are two factors to this magnification. The first comes from the ideal transfer function and predicts that the extent of the pattern in y should scale as $\sqrt{\alpha}$ to the lowest order, and the experimental data bears out this scaling. The second magnification is a scaling in x that is not predicted by the transfer function. We attribute this scaling to the cone angle of the source, which was not incorporated in the original derivation. The expansion comes from the cone angle acting over the path length of the on-axis ion trajectory. We show in the SI that the path length scales as $\alpha^{1/4}$ to lowest order. We would then expect to observe a functional dependence on the magnification in x and, again, the data bears this out. We do

not observe a noticeable contribution the magnification in y from this effect. We attribute this to the motion in y being dominated by interaction with the magnetic field, while motion in x is truly ballistic. We empirically incorporate this additional x -magnification M_x in the propagation kernel of Equation 3 with the substitution $x - x' \rightarrow x - (1 + M_x \alpha^{1/4})x'$ to yield the new propagation kernel:

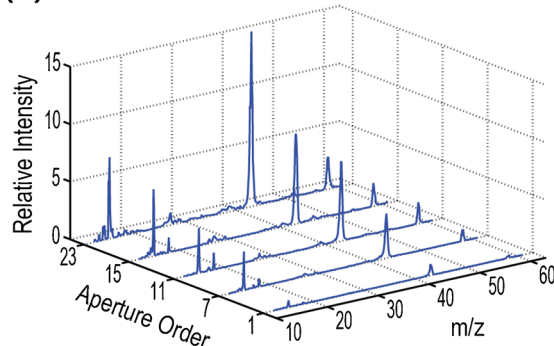
$$h(x, x', y, y', \alpha) \approx \delta \left(x - \left(1 + M_x \alpha^{1/4} \right) x', y - \sqrt{\frac{8U\alpha(u/e)}{B}} y' - y'^2 \right), \quad (5)$$

With this change, the remaining non-ideality is related to the accuracy of the assumptions that went into the derivation of the propagation kernel (e.g., normal incidence on the aperture, uniform magnetic field, etc.). Of the system parameters in the model, U , B , M_x , and Δ (the effective pixel sampling pitch size, see SI) we only know one (U) to a high degree of precision from an independent stopping potential experiment. Setting U to the measured value $U = 2$ kV, we seek a set of parameter values for B , M_x , and Δ which, when used in the discretized version of system transfer function, produce the best

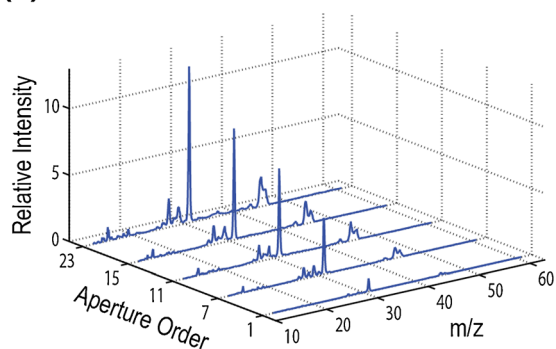
(a) Argon Reconstruction



(b) Acetone Reconstruction



(c) Ethanol Reconstruction



(d)

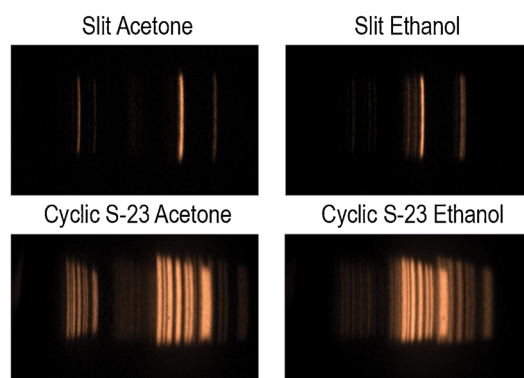


Figure 3. Reconstructed mass spectra results for argon, acetone, and ethanol for different aperture orders, and some representative unprocessed acetone and ethanol measurement images. (a)–(c) The reconstructed mass spectra across different aperture orders for argon (a), acetone (b), and ethanol (c) at a chamber pressure of $10.0 \mu\text{Torr}$ are presented. (d) Representative images obtained from acetone and ethanol at $10.0 \mu\text{Torr}$, illustrating the complexity of the data prior to reconstruction. The images are $40 \text{ mm} \times 10 \text{ mm}$

correspondence with the observed $m/z = 20$ and $m/z = 40$ patterns in Figure 2b. With the parameter values known, the discretized transfer function can then be estimated for all α . The resulting vectors are placed in the corresponding columns of the discretized system forward model matrix H (Equation 4). Because of the non-idealities, the parameter values extracted via this model-based approach do not exactly match the true experimental values (accurate to within a factor of two to five). However, they sufficiently balance the non-idealities to enable accurate quantitative reconstruction of the spectra as seen herein by the strong agreement between the reconstructed spectra and the library spectra for the various chemicals.

Experimental Results

In order to verify the forward model and reconstruction approach a series of mass-dispersed patterns of the coded apertures shown in Figure 1a, were obtained using the 90° MS described in [10] and shown in Figure 1b. Additional details on the sector, ion source, and ion detector appear in the SI. The apertures used were based on 1D Cyclic S codes [42] with a minimum feature size of $125\ \mu\text{m}$. Analytes of argon, acetone, and ethanol were introduced into the vacuum chamber containing the 90° MS via a bleed valve. Starting with a system base pressure of $0.5\ \mu\text{Torr}$, the analyte concentrations were varied by opening or closing the bleed valve to achieve pressures from 1.0 – $10.0\ \mu\text{Torr}$ in steps of $2.5\ \mu\text{Torr}$. This enabled the measurement of reproducible mass spectra consisting of only the analyte and residual water vapor across a wide range of concentrations. Detailed experimental procedures can be found in the SI.

Figure 3a–c show reconstructed spectra from argon, acetone, and ethanol versus aperture order. Each spectrum in this figure was taken at $10.0\ \mu\text{Torr}$. Representative detector images from which these spectra were reconstructed are shown in Figure 3d for acetone and ethanol. The relative intensity for each spectrum is normalized to the spectrum obtained from the slit (i.e., coded aperture order of one) to demonstrate the throughput gain achieved with the higher order coded apertures. Increasing aperture order is associated with significant improvement in throughput gain as seen by the increasing relative peak heights. Figure 3d illustrates the complexity of the collected data prior to reconstruction, including the overlapping images of individual coding elements, for an analyte containing multiple m/z species after ionization.

The experimentally realized throughput gain as a function of aperture order N is shown in Figure 4a. The throughput gain is calculated by computing the ratio of the area under the strongest reconstructed peak for each analyte and aperture order to that of the area of the corresponding peak for a slit aperture. The values presented in Figure 4a are the average gain across the three analytes and five pressures for each aperture order. The theoretical expectation is given by the ratio of total open area of the coded aperture to that of a single slit, and can be written as $(N + 1)/2$. This trend is also shown in Figure 4a for

purposes of comparison. The experimental throughput gain of different Cyclic S code orders follows the theoretical gain trend closely and the differences are likely a result of deviations from an ideal coded aperture (e.g., from over-etching of the aperture openings) and/or non-uniformities in the ion beam spatial profile. Furthermore, increasing aperture order does not affect the widths of the mass peaks, indicating that the resolution is maintained despite an increase in throughput of more than one order of magnitude. Figure 4b demonstrates that the effective resolution of the system is unaffected by the aperture coding approach, as both the S-23 and slit primary ethanol peaks at $m/z = 31$ have a full width at half maximum (FWHM) of $0.3\ m/z$.

An increase in throughput also leads to an improvement in the SBR, as expected. Figure 5a and b show a comparison of reconstructed slit and Cyclic S-23 ethanol mass spectra

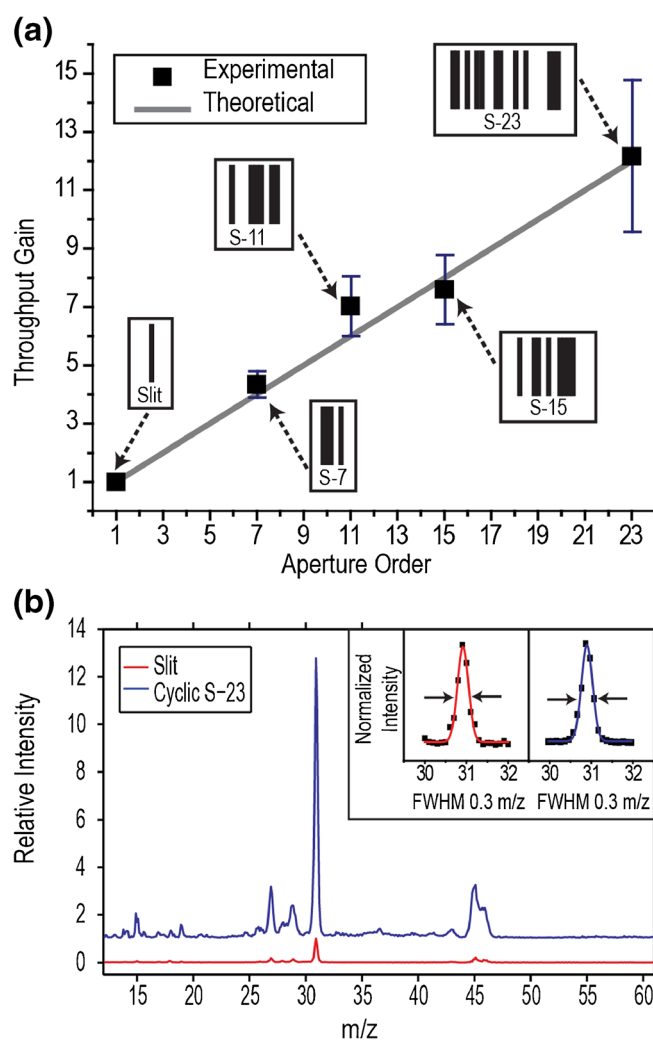


Figure 4. Throughput gain versus aperture order and resolution. (a) Plot of the average throughput gain over all pressures and analytes versus coded aperture order. The solid grey line indicates the expected throughput gain based on the open area of the apertures. (b) S-23 apertures show equivalent resolution to the slit with greater than 10X throughput as demonstrated by the FWHM (inset) of the primary ethanol peak at $m/z = 31$

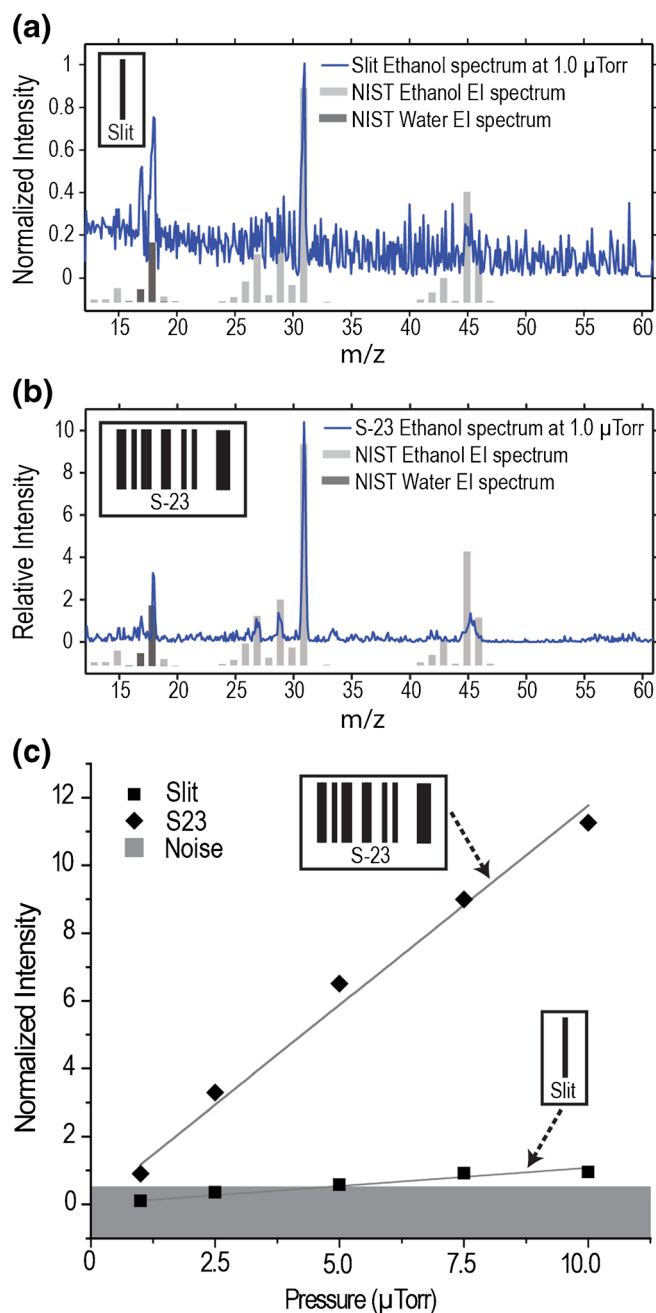


Figure 5. SBR and detection limit improvements with coded apertures. (a)–(b) are a comparison of normalized reconstructed spectra from low concentrations of ethanol (system pressure 1.0 μTorr) with NIST standards [43]. The system utilizing the slit aperture cannot resolve low intensity peaks such as those from $m/z = 26$ – 30 , and 45 – 46 . The system with the Cyclic S-23 coded aperture can detect these peaks found in the NIST standard spectrum above the background. (c) Intensity versus pressure comparison of coded apertures of order 1 (slit) and order 23 (Cyclic S-23) shows improvement in the detection limit of the instrument by an order of magnitude, as indicated by the increase in the slopes of pressure versus intensity curves. (Slit slope 1.08, S-23 slope 11.7, a difference of 10.9X). The grey band below a normalized intensity of 5 represents an “example noise floor” below which individual mass peaks cannot be positively detected

overlaid on the standard electron ionization mass spectra for ethanol and water from the NIST database [43]. At low analyte concentrations (i.e., a pressure of 1.0 μTorr), the slit spectrum does not reveal low intensity peaks such as those between $m/z = 26$ – 30 and $m/z = 45$ – 46 . However, the reconstructed spectrum from the Cyclic S-23 aperture is able to detect these peaks above the background. This is clear evidence of the improved SBR arising from the coded apertures.

Detection limits are another critical figure of merit when considering the analytical capabilities of a mass spectrometer. Depending on the noise level of the measurement system, there is some partial pressure of analytes that will not be detectable above the noise floor. In Figure 5c, ion signal intensity versus pressure data for the primary ethanol peak at $m/z = 31$ are shown for both the slit and S-23 apertures. The point where the pressure versus intensity trends intersect the noise floor of the system (the noise could be from any number of system factors) indicates the point at which the analyte would no longer be positively detected by the instrument. The slopes of the ion intensity versus pressure graphs increase with increasing aperture order, indicating improved detection limits from the use of spatially coded apertures. Specifically, for aperture order 23, an order of magnitude increase in slope is observed compared with the order 1 (slit) performance. This results in a similar increase in the instrument detection limits. This is illustrated in Figure 5c by an example noise floor arbitrarily placed at a normalized intensity of 5. In this situation, the normalized ion intensity of a slit aperture system drops below the noise floor at analyte pressures below 5.0 μTorr , indicating the loss of detection capability, whereas a system with an S-23 aperture would retain detection capability at an order of magnitude lower partial pressure of the analyte.

Discussion and Conclusions

Building on the analogy between optical spectroscopy and magnetic sector mass spectrometry, we have constructed a 90° magnetic sector mass spectrometer that demonstrates more than an order of magnitude improvement in throughput using spatially coded apertures. We have also derived a generalized forward model that can be applied to any sector instrument. We then applied this model to our 90° MS to develop a reconstruction algorithm. With this algorithm, we reconstructed mass spectra of argon, acetone, and ethanol from data collected using various coded apertures. The resulting throughput gains exceeded an order of magnitude and led to similarly increased SBR and lower detection limits while simultaneously maintaining the resolution of the slit instrument.

In this paper, we have demonstrated successful reconstruction of the mass spectra of argon, acetone, and ethanol—compounds with relatively simple mass spectra. However, results from optical spectroscopy have demonstrated that complicated spectra can be reconstructed in similar coded aperture approaches [14, 15, 44]. The interplay of noise, resolution, accuracy of the forward model, and performance of the

inversion techniques is a complicated process that will determine the ultimate accuracy of the reconstruction of mass spectra for more complex compounds and is a topic of ongoing research in our and other laboratories.

The maximum resolving power of our system is related to the minimum feature size of the aperture. In our demonstration, we fabricated the slit and coded apertures with identical feature sizes so that resolving power was constant. As a result, the open area (and hence the throughput) of the coded aperture systems was increased. Conversely, we could have fabricated the coded apertures such that their open area (throughput) was equal to that of the slit. This would have increased the resolving power of the coded aperture systems (subject to limitations imposed by other aspects of the system—ion optic aberrations, dispersion, etc.)

Finally, we expect that applying spatial coding concepts to other sector instruments, such as double focusing sector geometries, will also overcome the throughput versus resolution tradeoff and enable miniaturization without the accompanying loss in performance. This is the subject of ongoing work.

Acknowledgments

This work was performed with partial support of the US Department of Homeland Security's Science and Technology Directorate (Contract HSHQDC-11-C-00082). Initial development of the system algorithms utilized in this research was supported by the National Science Foundation (Contract ECCS-0801942). The authors also thank the Shared Materials Instrumentation Facility at Duke and Dr. James (Mitch) Wells for useful discussions.

References

- McLuckey, S.A., Wells, J.M.: Mass analysis at the advent of the 21st century. *Chem. Rev.* **101**(2), 571–606 (2001)
- McLafferty, F.W.: A century of progress in molecular mass spectrometry. *Ann. Rev. Anal. Chem.* **4**(1), 1–22 (2011)
- Biemann, K.: Mass spectrometry of peptides and proteins. *Ann. Rev. Biochem.* **61**(1), 977–1010 (1992)
- Richardson, S.D.: Mass spectrometry in environmental sciences. *Chem. Rev.* **101**(2), 211–254 (2001)
- Badman, E.R., Graham Cooks, R.: Miniature mass analyzers. *J. Mass Spectrom.* **35**(6), 659–671 (2000)
- Ouyang, Z., Cooks, R.G.: Miniature mass spectrometers. *Ann. Rev. Anal. Chem.* **2**(1), 187–214 (2009)
- Palmer, P.T., Limero, T.F.: Mass spectrometry in the U.S. space program: past, present, and future. *J. Am. Soc. Mass Spectrom.* **12**(6), 656–675 (2001)
- Diaz, J., Giese, C., Gentry, W.R.: Sub-miniature ExB sector-field mass spectrometer. *J. Am. Soc. Mass Spectrom.* **12**(6), 619–632 (2001)
- Sinha, M.P., Wadsworth, M.: Miniature focal plane mass spectrometer with 1000-pixel modified-CCD detector array for direct ion measurement. *Rev. Sci. Instrum.* **76**, 025103 (2005)
- Russell, Z., Chen, E., Amsden, J., Wolter, S., Danell, R., Parker, C., Stoner, B., Gehm, M., Brady, D., Glass, J.: Two-dimensional aperture coding for magnetic sector mass spectrometry. *J. Am. Soc. Mass Spectrom.* **26**(2), 248–256 (2015)
- Felton, J.A., Schilling, G.D., Ray, S.J., Sperline, R.P., Denton, M.B., Barinaga, C.J., Koppelaar, D.W., Hieftje, G.M.: Evaluation of a fourth-generation focal plane camera for use in plasma-source mass spectrometry. *J. Anal. At. Spectrom.* **26**(2), 300–304 (2011)
- Hadjar, O., Johnson, G., Laskin, J., Kibelka, G., Shill, S., Kuhn, K., Cameron, C., Kassan, S.: IonCCD for direct position-sensitive charged-particle detection: from electrons and keV ions to hyperthermal biomolecular ions. *J. Am. Soc. Mass Spectrom.* **22**(4), 612–623 (2011)
- Brady, D.J.: *Optical imaging and spectroscopy*. John Wiley and Sons, Hoboken, NJ (2009)
- McCain, S.T., Gehm, M.E., Wang, Y., Pitsianis, N.P., Brady, D.J.: Coded aperture Raman spectroscopy for quantitative measurements of ethanol in a tissue phantom. *Appl. Spectrosc.* **60**(6), 663–671 (2006)
- Gehm, M.E., McCain, S.T., Pitsianis, N.P., Brady, D.J., Potuluri, P., Sullivan, M.E.: Static two-dimensional aperture coding for multimodal, multiplex spectroscopy. *Appl. Opt.* **45**(13), 2965–2974 (2006)
- Eckhardt, C.J., Gross, M.L.: A proposed technique for signal multiplexing in mass spectrometry. *Int. J. Mass. Spectrom. Ion. Phys.* **5**(3/4), 223–227 (1970)
- Brock, A., Rodriguez, N., Zare, R.N.: Hadamard transform time-of-flight mass spectrometry. *Anal. Chem.* **70**(18), 3735–3741 (1998)
- Zare, R.N., Fernández, F.M., Kimmel, J.R.: Hadamard transform time-of-flight mass spectrometry: more signal, more of the time. *Angew. Chem. Int. Ed.* **42**(1), 30–35 (2003)
- Trapp, O., Kimmel, J.R., Yoon, O.K., Zuleta, I.A., Fernandez, F.M., Zare, R.N.: Continuous two-channel time-of-flight mass spectrometric detection of electrosprayed ions. *Angew. Chem. Int. Ed.* **43**(47), 6541–6544 (2004)
- Williams, E.R., Loh, S.Y., McLafferty, F.W., Cody, R.B.: Hadamard transform measurement of tandem Fourier-transform mass spectra. *Anal. Chem.* **62**(7), 698–703 (1990)
- Bushey, J.M., Danell, R.M., Glish, G.L.: Iterative accumulation multiplexing Fourier transform ion cyclotron resonance mass spectrometry. *Anal. Chem.* **81**(14), 5623–5628 (2009)
- Chen, E., Gehm, M., Danell, R., Wells, M., Glass, J., Brady, D.: Compressive mass analysis on quadrupole ion trap systems. *J. Am. Soc. Mass Spectrom.* **25**(7), 1295–1304 (2014)
- Paul, W., Steinwedel, H.: A new mass spectrometer without a magnetic field. *Zeitschrift fuer Naturforschung (West Germany) Divided into Z. Naturforsch., A, and Z. Naturforsch. B. Anorg. Chem., Org. Chem., Biochem., Biophys.* **8**, 448–450 (1953)
- Louris, J.N., Cooks, R.G., Syka, J.E.P., Kelley, P.E., Stafford, G.C., Todd, J.F.J.: Instrumentation, applications, and energy deposition in quadrupole ion-trap tandem mass spectrometry. *Anal. Chem.* **59**(13), 1677–1685 (1987)
- March, R.E.: An introduction to quadrupole ion trap mass spectrometry. *J. Mass Spectrom.* **32**(4), 351–369 (1997)
- Wolff, M.M., Stephens, W.E.: A pulsed mass spectrometer with time dispersion. *Rev. Sci. Instrum.* **24**(8), 616–617 (1953)
- Wiley, W.C., McLaren, I.H.: Time-of-flight mass spectrometer with improved resolution. *Rev. Sci. Instrum.* **26**(12), 1150–1157 (1955)
- Brown, R.S., Lennon, J.J.: Mass resolution improvement by incorporation of pulsed ion extraction in a matrix-assisted laser desorption/ionization linear time-of-flight mass spectrometer. *Anal. Chem.* **67**(13), 1998–2003 (1995)
- Beauchamp, J.L.: Ion cyclotron resonance spectroscopy. *Ann. Rev. Phys. Chem.* **22**(1), 527–561 (1971)
- Comisarow, M.B., Marshall, A.G.: The early development of Fourier transform ion cyclotron resonance (FT-ICR) spectroscopy. *J. Mass Spectrom.* **31**(6), 581–585 (1996)
- Marshall, A.G.: Milestones in Fourier transform ion cyclotron resonance mass spectrometry technique development. *Int. J. Mass. Spectrom.* **200**(1/3), 331–356 (2000)
- Dempster, A.: A new method of positive ray analysis. *Phys. Rev.* **11**(4), 316–325 (1918)
- Stephens, W.E.: Magnetic refocussing of electron paths. *Phys. Rev.* **45**(8), 513–518 (1934)
- Nier, A.O.: A mass spectrometer for routine isotope abundance measurements. *Rev. Sci. Instrum.* **11**(7), 212–216 (1940)
- Mattauch, J., Herzog, R.: Über einen neuen Massenspektrographen. *Z. Physik.* **89**(11/12), 786–795 (1934)
- Williams, D.H., Fleming, I.: *Spectroscopic methods in organic chemistry*. McGraw-Hill, London (1980)
- Bainbridge, K.T., Jordan, E.B.: Mass Spectrum analysis 1. The mass spectrograph 2. The existence of isobars of adjacent elements. *Phys. Rev.* **50**(4), 282–296 (1936)
- Bleakney, W., Hipple Jr., J.A.: A new mass spectrometer with improved focusing properties. *Phys. Rev.* **53**(7), 521–529 (1938)
- Aston, F.W.: LXXIV. A positive ray spectrograph. *Philos. Mag. Series 6* **38**(228), 707–714 (1919)

40. Ligon, W.V.: Molecular analysis by mass spectrometry. *Science* **205**(4402), 151–159 (1979)
41. Richardson, W.H.: Bayesian-based iterative method of image restoration. *J. Opt. Soc. Am.* **62**(1), 55–59 (1972)
42. Harwit, M.: Hadamard transform optics. Academic Press, Waltham, MA (1979)
43. Linstrom, P.J., Mallard, W.G. (eds.): NIST Chemistry WebBook, NIST Standard Reference Database Number 69. National Institute of Standards and Technology, Gaithersburg, MD, 20899 (2005)
44. Gehm, M.E., Hsieh, C., Feller, S.D., Chen, H., Momtahan, O., Adibi, A., Brady, D.J.: Multiple order coded aperture spectrometer. *Opt. Express* **15**(9), 5625–5630 (2007)